# Highly Luminescent Phase-Stable $CsPbI_3$ Perovskite Quantum Dots Achieving Near 100% Absolute Photoluminescence Quantum Yield

Feng Liu,[1] Yaohong Zhang,[1] Chao Ding,[1] Syuusuke Kobayashi,[1] Takuya Izuishi,[1] Naoki Nakazawa,[1] Taro Toyoda,[1,6] Tsuyoshi Ohta,[2] Shuzi Hayase,[2,6] Takashi Minemoto,[3,6] Kenji Yoshino,[4,6] Songyuan Dai,[5] and Qing Shen*,[1,6]

[1]Faculty of Informatics and Engineering, The University of Electro-Communications, 1-5-1 Chofugaoka, Chofu, Tokyo 182-8585, Japan

[2]Faculty of Life Science and Systems Engineering, Kyushu Institute of Technology, 2-4 Hibikino, Wakamatsu-ku, Kitakyushu, Fukuoka 808-0196, Japan

[3]Department of Electrical and Electronic Engineering, Faculty of Science and Engineering, Ritsumeikan University, 1-1-1 Nojihigashi, Kusatsu, Shiga 525-8577, Japan

[4]Department of Electrical and Electronic Engineering, Miyazaki University, 1-1 Gakuen, Kibanadai Nishi, Miyazaki 889-2192, Japan

[5]Beijing Key Laboratory of Novel Thin Film Solar Cells, State Key Laboratory of Alternate Electrical Power System with Renewable Energy Sources, North China Electric Power University, Beijing, 102206, P. R. China

[6]CREST, Japan Science and Technology Agency (JST), 4-1-8 Honcho, Kawaguchi, Saitama 332-0012, Japan

Email: shen@pc.uec.ac.jp

**Abstract**

Perovskite quantum dots (QDs) as a new type of colloidal nanocrystals have gained significant attention for both fundamental research and commercial applications owing to their appealing optoelectronic properties and excellent chemical

processability. For their wide range of potential applications, synthesizing colloidal QDs with high crystal quality is of crucial importance. However, like most common QD systems such as CdSe and PbS, those reported perovskite QDs still suffer from a certain density of trapping defects, giving rise to detrimental non-radiative recombination centers and thus quenching luminescence. In this paper, we show that a high room-temperature photoluminescence quantum yield of up to 100% can be obtained in $CsPbI_3$ perovskite QDs, signifying the achievement of almost complete elimination of the trapping defects. This is realized with our improved synthetic protocol that involves introducing organolead compound trioctylphosphine-$PbI_2$ (TOP-$PbI_2$) as the reactive precursor, which also leads to a significantly improved stability for the resulting $CsPbI_3$ QD solutions. Ultrafast kinetic analysis with time-resolved transient absorption spectroscopy evidences the negligible electron or hole trapping pathways in our QDs, which explains such a high quantum efficiency. We expect the successful synthesis of the "ideal" perovskite QDs will exert profound influence on their applications to both QD-based light-harvesting and -emitting devices.

**Keywords:** cesium lead halide perovskite nanocrystals, 100% photoluminescence quantum yield, perovskite quantum dot, stable perovskite, colloidal nanoparticles

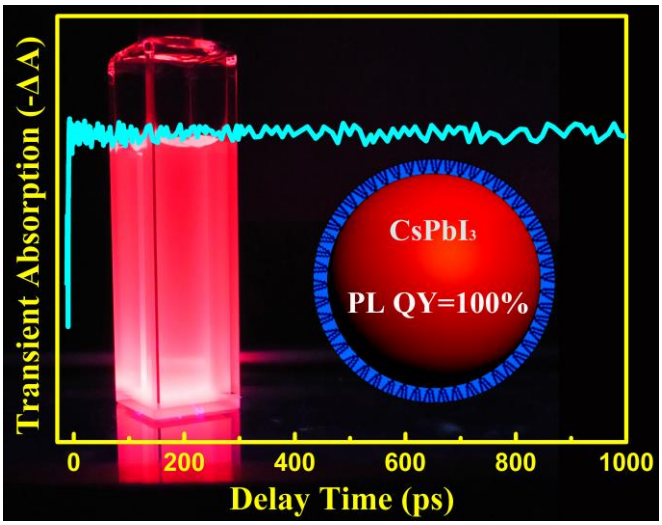

TOC

Various properties of all-inorganic cesium lead halide perovskite ($CsPbX_3$, X = Cl, Br, I, and mixed Cl/Br and Br/I) quantum dots (QDs), including size-tunable band gap, high photoluminescence (PL) quantum yield (QY), narrow emission peak widths, and improved air stability (contrary to $CH_3NH_3PbX_3$), render these materials extremely attractive for a range of potential applications, such as solar cells, light emitting diodes, photodetectors, and lasers.[1-8] In 2015, Kovalenko and co-workers synthesized highly luminescent $CsPbX_3$ QDs using a hot-injection method, wherein Cs-oleate was swiftly injected into an octadecene (ODE) solution containing $PbI_2$, oleic acid (OA), and oleylamine (OAm) (hereafter refer to as standard "OA/m" route).[9] The resulting nanocrystals have nearly perfect surface stoichiometry and narrow size distribution. More recently, following the success of colloidal synthesis, appealing optoelectronic properties were revealed for $CsPbBr_3$ QDs, such as remarkably high carrier mobility (~4500 $cm^2V^{-1}$ $s^{-1}$), large diffusion length (>9.2 μm), and ultrafast interfacial charge transfer, which further highlight their prospective use in photoelectric devices.[10-12] Its iodine analogue, $CsPbI_3$, should be of more interest for solar cell applications because the light absorption of $CsPbI_3$ can exceed 700 nm by virtue of its narrower band gap (~1.73 eV for bulk $CsPbI_3$) than either $CsPbBr_3$ (~2.25 eV) or $CsPbCl_3$ (~3.05 eV).[13, 14] In fact, an inspiring solar-energy conversion efficiency as high as 10.77% has recently been achieved for $CsPbI_3$ QD solar cells.[1] However, in comparison with the well-established $CsPb(Cl/Br)_3$ and $CH_3NH_3PbX_3$ optical systems, fundamental researches on $CsPbI_3$ QDs are not as advanced. One of the main reasons might be due to the difficulty in preparing $CsPbI_3$ nanocrystals with stable cubic perovskite phase. It was found that in standard OA/m route the resulting $CsPbX_3$ QDs are dynamically stabilized with both long chain carboxylic and oleyammonium surface ligands.[1, 12, 15] While, in the case of $CsPbI_3$ QDs, those of ammonium ligands can be easily lost during the routine but essential purification procedures because of the weak acid-base interactions between $I^-$ and oleylammonium, causing a fast agglomeration and an

undesired phase transformation from cubic to orthorhombic. In unpurified solution, it was observed that the QDs can still undergo such a degradation, which is primarily caused by a reaction with an excess of amines.[12] A recent breakthrough was achieved by utilizing methyl acetate (MeOAc) as the anti-solvent during QD extraction, which has proven beneficial in stabilizing the cubic phase as it minimized the surfactant loss of the QDs, leading to a high photovoltaic efficiency achieved for $CsPbI_3$ QD solar cells.[1] However, like most common QD systems such as CdSe and PbS, a certain density of trapping defects still exist in those resulting perovskite QDs as evidenced by their maximum PL QYs of ~80% less than 100%.[1,8] Trap states of the QDs significantly influence their optical and optoelectronic properties and consequently, the device performance.[16, 17] For instance, when the QDs are applied in solar cells, the high density of defects in QD active layers will deteriorate the photovoltaic efficiency because the defects act as the recombination centers of the charge carriers.[18, 19] Similarly, in light-emitting devices, defects of the QDs create non-radiative recombination pathways that limit the efficiency of radiation.[20-23] Hence, considerable scope remains for further enhancement in photovoltaic performance and photoluminescence efficiency if trapping defects of these synthesized $CsPbI_3$ QDs are completely eliminated. Yet it should be noted that although colloidal synthesis of nanocrystals has developed for decades of years, it is still challenging to synthesize QDs with a perfect crystal structure and complete defect elimination.[24-27]

Trioctylphosphine (TOP) as a kind of alkylphosphine is a commonly used coordinating solvent during the synthesis of II-VI, III-V, and IV-VI nanocrystals, for example, CdX (X=S, Se, Te), InP, PbS, and PbSe QDs.[28-33] Due to the presence of lone pair electrons on the phosphorus atom, TOP possesses strong solvent ability toward both selenium and sulfur powder, thus oil-soluble anion precursors TOP-X can be facilely prepared. It is also generally thought that the TOP species can coordinate to the surface of the resulting QDs through a certain scheme, supplying a more complete surface passivation for the QDs.[34-38] In this paper, we demonstrate that the warm TOP solution can readily dissolve $PbI_2$ powder, forming stable and highly

reactive $PbI_2$ precursor that can be used for the synthesis of high-quality $CsPbI_3$ QDs with extremely high luminescence and enhanced chemical stability. The size of the QDs can be controlled by changing the reaction temperature during the synthesis. PL QY efficiency of the purified QDs as high as nearly 100% is achieved for different-sized QDs. Time-resolved photoluminescence study reveals a much longer photoexcited exciton lifetime in our QDs than the previous ones, which points to a significant reduction of the quenching defects. To further elucidate the mechanism of the superior PL QYs of the TOP route-prepared $CsPbI_3$ QDs, we have also carried out ultrafast exciton dynamic study using transient absorption (TA) spectroscopy, which indicates the negligible electron or hole trapping pathways in the resulting QDs. Our findings thus lay the foundation for understanding the fundamental physics behind these amazing QDs.

## Results and discussion

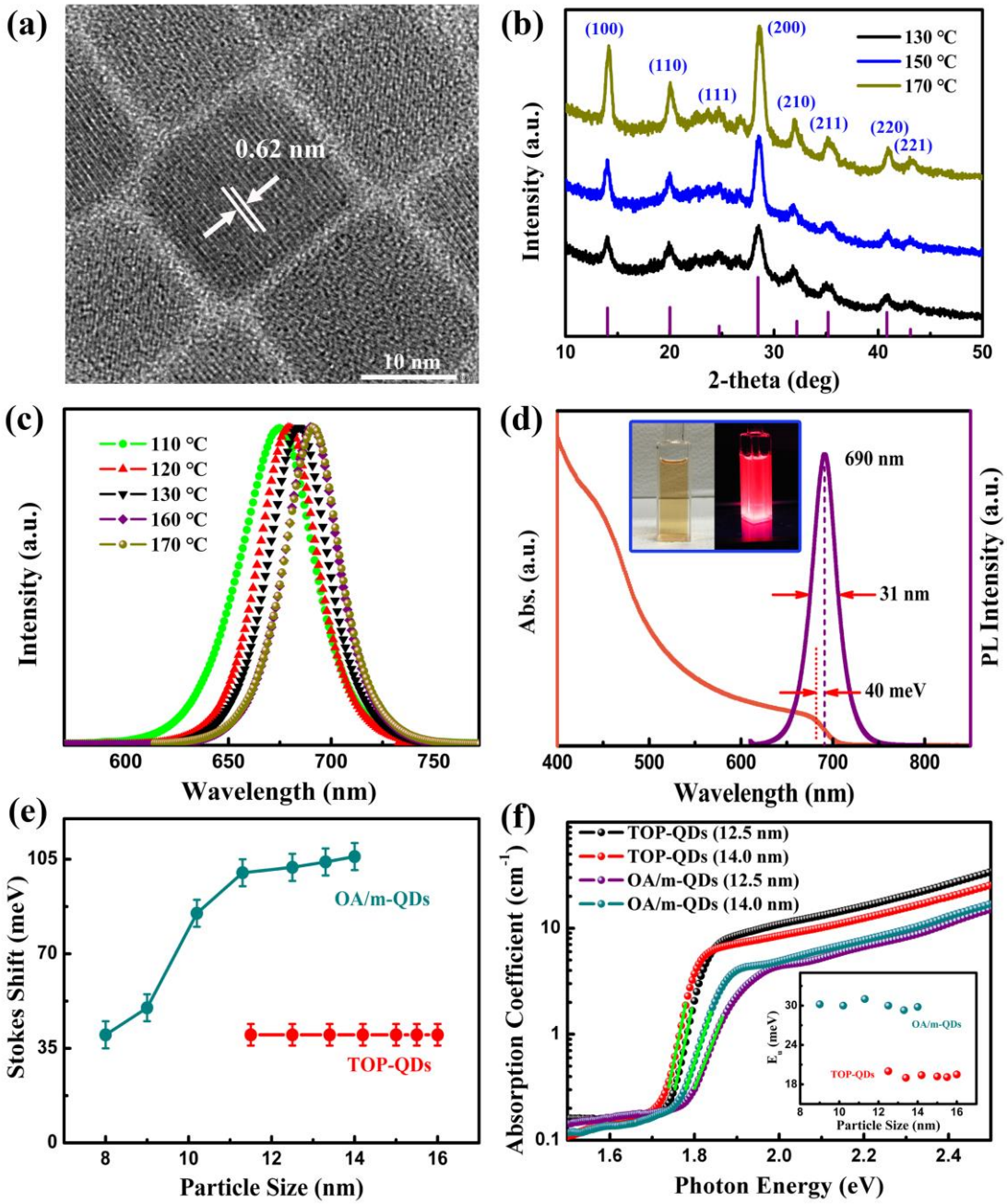


**Figure 1.** (a) HRTEM image of the colloidal $CsPbI_3$ QDs prepared under 160 °C. (b) XRD patterns of $CsPbI_3$ QDs synthesized at different temperatures. The vertical bars represent the position of the diffraction peaks for the bulk cubic $CsPbI_3$ lattice structure, and their lengths are proportional to their intensity. XRD samples are prepared by directly depositing purified QD suspension on a pre-cleaned glass substrate and dried by spin-casting at 1,500 r.p.m. for 20 s. (c) Steady-state PL emission spectra for a series of $CsPbI_3$ QDs synthesized at different temperatures. From left to right, the PL emission maxima/FWHM of the samples are 673 nm/39 nm,

679 nm/35 nm, 684 nm/33 nm, 690 nm/31 nm, and 692 nm/31 nm, respectively. (d) UV-vis absorption and PL spectra of $CsPbI_3$ QDs prepared under 160 °C, where the Stokes shift energy is 40 meV. The inset shows the photos of the QD solution under the room light (left) and bright red luminescence of the QD solution upon irradiation with a UV lamp ($\lambda$ = 365 nm) (right). (e) Dependence of the Stokes shift of the TOP- and OA/m-$CsPbI_3$ QDs on their particle sizes. (f) Optical absorption spectra of the different-sized TOP- and OA/m-$CsPbI_3$ QDs. The inset shows the corresponding Urbach energies for these two kinds of QDs with different sizes.

In a typical synthesis of $CsPbI_3$ QDs using the method proposed by us, an ODE solution containing OA, OAm, and Cs-oleate was heated to 100-170 °C followed by the swift injection of a solution of TOP-$PbI_2$ (more experimental details about the synthesis of the QDs can be found in Methods section, QDs prepared are thus denoted as "TOP-QDs"). Purification of the crude as-synthesized QDs was carried out with the recently developed washing process using anti-solvent MeOAc.[1] To clearly guide the readers, we photographed every single step of our washing process, as shown in Figure S1. Attempts to synthesize $CsPbBr_3$ or $CsPbCl_3$ QDs using the same reaction scheme, however, failed, due to the extremely low solubility of $PbBr_2$ and $PbCl_2$ in the pure TOP reagent (<< 0.1 mol/L, even at elevated temperatures). In fact, we found that $PbI_2$ concentrations $\geq$ 0.5 mol/L are required to run the successful synthesis of the stable $CsPbI_3$ QDs. Particle size of the resulting $CsPbI_3$ QDs can be tuned by the choice of injection temperature, typically ranging from ~11 to 16 nm. Figure S2 shows the size and shape of the TOP-QDs synthesized at various temperatures using high-resolution transmission electron microscopy (HRTEM). Figure 1a gives a representative HRTEM image of the product synthesized at 160 °C, revealing the presence of rather monodisperse cubic-shaped QDs with high crystallinity. Figure S3 shows high-resolution X-ray photoelectron spectroscopy (XPS) spectra taken of the Cs, Pb, and I regions for TOP-QDs. The measured binding energies at 723.9 eV and 138.5 eV can be well assigned to Cs(I) and Pb(II), respectively, which are in

agreement with values of perovskite in literature.[39, 40] Particularly, the I 3d5/2 spectrum of the TOP-QD sample can be well deconvoluted into two peaks located at 619.5 eV and 618.4 eV, corresponding to the contribution from Pb-I and Cs-I interactions, respectively.[41, 42] XRD patterns of the resulting QDs shown in Figure 1b can be well indexed to the bulk cubic $CsPbI_3$.[9, 43-46] In particular, the measured interplanar spacing of 0.62 nm in the HRTEM corresponds to (100) plane of cubic phase of $CsPbI_3$. Increasing the reaction temperature yields very narrow XRD features which correspond to larger particle size. Figure S4 and Figure 1c show the optical absorption and PL spectra measured at room temperature for the different-sized QDs ranging from ~11 to 16 nm, respectively. As the size increases, the absorption spectra of the QDs show red shifts where the wavelength of the optical absorption peak increases from 668 to 684 nm. Note that the exact optical absorption peak for each size QD is determined from TA spectra using TA bleach peak measured under the low excitation intensity, see Figure S5. Simultaneously, the PL peak wavelength increases from 673 to 692 nm, along with a decrease in the full width at half maximum (FWHM) of the PL spectrum from 42 to 31 nm. The slightly increased absorption band edge indicates that our resulting $CsPbI_3$ QDs actually have a weak quantum confinement. This can be rationalized that particle size of these QDs (~11-16 nm) is actually very close to the exciton Bohr diameter (~13 nm) of $CsPbI_3$.[9] For comparison, reference $CsPbI_3$ QDs were also synthesized according to the standard OA/m route described in the literature (refer to as "OA/m-QDs").[9] A detailed spectra comparison in Figure S6 demonstrates that in contrast to OA/m synthesis, our TOP route typically yields larger QDs under the same reaction temperature, as evidenced by both obvious red shifts of the UV-vis absorption and PL spectra compared to those of OA/m-QDs. In fact, particle size of the TOP-$CsPbI_3$ QDs synthesized at 130 °C has already reached that of the OA/m-QDs synthesized at 160 °C (~13 nm), suggesting a much faster reaction rate and thus more active $PbI_2$ precursor in our TOP route. Larger QD size which corresponds to a wider spectral absorption is preferable for their photovoltaic applications. Moreover, like the presented QDs synthesized at 160 °C (Figure 1d),

small values of Stokes shift (~40 meV) are resolved in all spectra of the TOP-QDs with different particle sizes, which points to a direct band-edge radiative recombination process in the resulting QDs (Stokes shift is defined as the energy different between exciton absorption peak and emission peak).[47, 48] Values of the Stokes shift of the TOP-QDs were further compared to those of the OA/m-QDs in Figure 1e, which reveals much smaller Stokes shifts in the former. This result suggests that the photophysical properties of the resulting TOP-$CsPbI_3$ QDs have significantly changed from those of the QDs prepared by traditional methods. In fact, as a critical component in nanocrystal synthesis, the reactive precursors greatly influence the surface chemistry as well as control the nucleation and growth dynamics of the resulting nanocrystals, and eventually determine their physical and chemical properties.[49] In order to gain more insight about the superior photophysical properties of the TOP-$CsPbI_3$ QDs, we further investigate the Urbach energies in these two kinds of QDs by plotting their absorption coefficient as a function of photon energy (Figure 1f). In semiconductors and insulators, the fundamental absorption edge below the energy band gap increases exponentially, and the absorption edge is known as the Urbach tail.[50] Fitting the exponential part of the Urbach tail with the following Urbach's rule (eq. (1)) allows us to extract the Urbach energy ($E_U$), which represents the absorption tail states of these materials and is closely related to the degree of electronic disorder within the crystals.[50] A large $E_U$ value is a strong indicator that the samples suffer from a cumulative effect of impurities, inherent structural disorders, and electron-phonon interaction in the absorption processes.[51-53]

$$\alpha(E) = \alpha_0 \exp\left[ \sigma(T) \frac{E - E_0}{k_B T} \right] \quad (1)$$

where $\alpha(E)$ is the absorption coefficient as a function of photon energy $E$, $E_0$ and $\alpha_0$ are the characteristic parameters of the material, $\sigma(T)$ is the steepness parameter, $k_B$ is the Boltzmann constant, and $T$ is the absolute temperature. The Urbach energy is

defined as $E_U = k_BT/\sigma(T)$. Figure 1f shows the typical room-temperature logarithmic absorption coefficient of OA/m- and TOP-$CsPbI_3$ QDs as a function of photon energy, where unusual sharp optical band edges can be observed in both kinds of QDs. Urbach energies derived by fitting eq. (1) to the exponential tails shown in Figure 1f for both OA/m- and TOP-$CsPbI_3$ QDs are summarized in the inset of Figure 1f. Remarkably, TOP-$CsPbI_3$ QDs in all sizes have $E_U$ values varying from ~18 to 19 meV, while for OA/m-QDs, $E_U$ values are around 30 meV. This result indicates TOP-QDs have a lower level of electronic disorder and/or defect density compared to OA/m-QDs, and therefore better crystalline nature. In addition, the measured low Urbach energies for TOP-$CsPbI_3$ QDs are similar to those of bulk $CH_3NH_3PbI_3$ perovskites (~15 meV).[52] It is generally accepted that for an active light-absorbing material, the lower Urbach energy which corresponds to a superior electronic property is critical to achieving high open-circuit voltage for the solar cells.[51, 52]

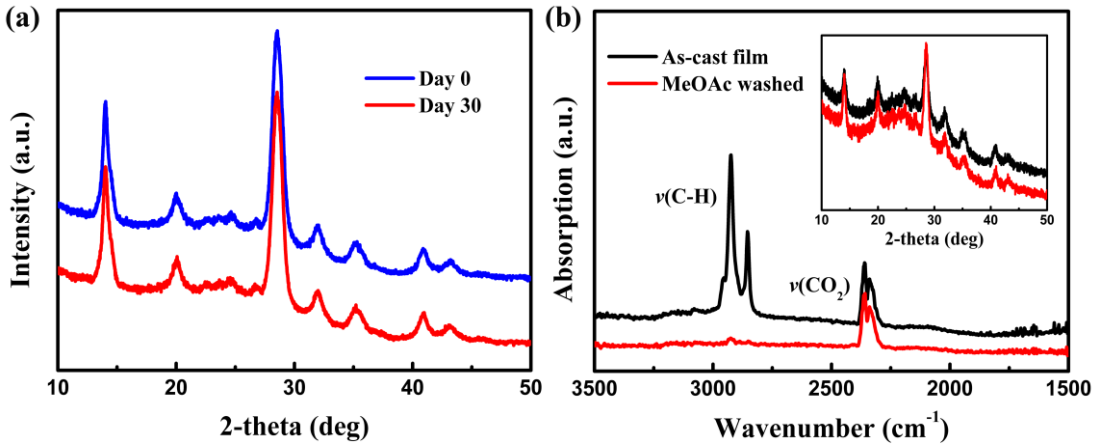


**Figure 2.** (a) XRD patterns of the fresh TOP-$CsPbI_3$ QDs synthesized at 160 °C and those stored under ambient conditions for 30 days (both are purified twice with MeOAc). (b) FT-IR absorption spectra showing the IR absorption of a TOP-$CsPbI_3$ QD film as cast on a glass substrate (black) and after flooding the surface with MeOAc (red). Inset shows thin film XRD patterns of the two samples.

Colloidal stability of a QD solution is of particular importance for both fundamental and applied researches. However, the standard OA/m route normally

yields unstable $CsPbI_3$ QDs if just the routine washing method is employed.[1, 54] Remarkably, TOP-QDs can be kept stable and maintain an excellent dispersibility in non-polar solvent irrespective of the washing methods involved in the purification process. Figure 2a shows XRD patterns of the fresh MeOAc-washed TOP-QDs (washed twice) and those after storage in solution for 1 month, which are the same, indicating no degradation of the TOP-QDs within this period of time. To clearly demonstrate this advantage, in Table S1, we summarized and compared samples of TOP-QDs and OA/m-QDs with respect to their colloidal stability under the same washing treatment after synthesis. Obviously, OA/m-QDs could only exhibit stable phase with MeOAc washing, while those butanol-washed or crude samples degrade into orthorhombic phase after storage for 2-3 days, consistent with the previous observations.[1, 54] In contrast, with either butanol washing or in crude solution (diluted with hexane), TOP-QDs maintain a stable cubic phase during a continuous 1-month observation period. The excellent stability of the purified TOP-QD solution is considered to result from the conservation of those protective alkylammonium oleate ligands around QDs (as discussed later), which prevents QDs from aggregation. Additionally, we have made a detailed comparison of the UV-vis absorption and PL spectra between the as-synthesized QDs with that of the purified samples since previous studies indicate that anti-solvent washing may have a large impact on optical properties of the resulting QDs.[55, 56] As shown in Figure S7, for those reference OA/m-QDs, we found a ~15 nm red shift in both absorption and PL spectra between the as-synthesized product and the anti-solvent purified samples. Similar observation can be found in previous reports on $CsPbBr_3$ QDs and can be attributed to the loss of part of the surface ligands, which causes nonnegligible agglomeration and fusion of the QDs.[55, 56] While, interestingly, for TOP-QDs, such red shift is relatively lower, being ~3.4 nm, suggesting a better ligand protection for the resulting QDs.

However, we also note the fact that although our washed $CsPbI_3$ QDs maintain an excellent stability in colloidal solution, they still become less stable after evaporating their solvent and directly exposed to the open air (the ambient relative humidity was

40-60%, 20 °C). Figure S8 shows thin film XRD patterns of the $CsPbI_3$ QDs after storage in air and under ambient conditions for 3 days, at which point peaks characteristic of the orthorhombic phase appeared and became dominant over time. This observation is in accordance with Luther *et al.*'s report, in which a notable decrease in photovoltaic performance was recorded for OA/m-$CsPbI_3$ QD thin film solar cells after storage for 2 days in humid conditions.[1] It should be noted, additionally, that for both TOP- and OA/m-based route, $CsPbI_3$ QD thin films can be phase-stable when stored in a desiccator or a $N_2$-filled glove box, emphasizing the need for additional strategies to stabilize the cubic phase of $CsPbI_3$ QDs of solid films under humid conditions.

It is worth mentioning that the above prepared QD thin films for XRD measurement through spin casting and drying process still contain considerable amount of organic species, which militate against efficient carrier transport in semiconductor thin films, and thus decreasing the efficiency of the solar cells or LEDs.[57, 58] MeOAc washing proposed by Luther *et al.* has been demonstrated efficient in removing organic ligands from the surface of these $CsPbI_3$ QDs while retaining their desired cubic phase.[1] Here, we also employ this convenient method to explore the potential use of TOP-$CsPbI_3$ QDs in efficient thin film solar cells and LEDs. Figure 2b shows the FT-IR absorption spectra of a TOP-$CsPbI_3$ QD film as cast and after washing with MeOAc, which confirms the removal of most organic species in the washed sample as the strong C-H bending vibration peaks at 2853 and 2923 $cm^{-1}$ assignable to the hydrocarbon chains from those organics are much reduced. In addition, thin film XRD patterns of the samples shown in the inset figure indicate that the cubic phase of these washed QDs was intact. The above observations thus suggest that our colloidal TOP-$CsPbI_3$ QDs can be potentially processed into thin films for practical use in optoelectronics.

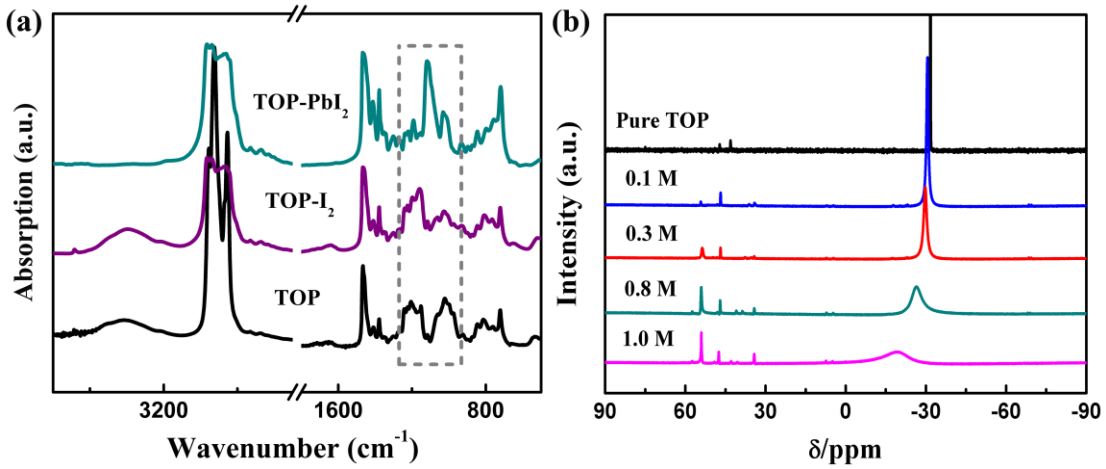


**Figure 3.** (a) FT-IR absorption spectra of TOP-$PbI_2$, TOP-$I_2$, and TOP. Samples were prepared by freezing their liquid solution at 4 ℃ for 1 hour. All FT-IR measurements were performed under ambient conditions. (b) $^{31}P$ NMR spectra of the TOP-$PbI_2$ complex solution with different $PbI_2$ concentrations. Samples are measured in Toluene-d8.

The successful synthesis of the phase-stable $CsPbI_3$ QDs enabled by TOP route inspired us to examine the nature of the intermediate formed during the dissolution of $PbI_2$ powder in TOP. This is also the key point and the major difference from that of the previous methods. Such a $PbI_2$ dissolution scheme in TOP might resemble that of DMSO·$PbI_2$, a high-profile $PbI_2$ adduct that is recently widely used for highly efficient perovskite solar cells. In the latter case, lone pair electrons on oxygen in DMSO donates to Lewis acid $Pb^{2+}$ in $PbI_2$, leading to the formation of reactive DMSO·$PbI_2$ adduct in DMSO solution.[59, 60] In order to investigate such an adduct in our TOP-$PbI_2$ system, we also performed Fourier transform infrared (FT-IR) spectroscopy on samples of TOP and TOP-$PbI_2$ (Figure 3a). First, it is shown that in contrast to the pure TOP species, the spectrum of the TOP-$PbI_2$ complex does not contain any O-H stretching absorption bands of water molecule at 3000-3600 $cm^{-1}$, indicating the product is highly water-resistant. Further, importantly, distinct from that of the pure TOP, there exists a strong absorption peak located at 1047-1142 $cm^{-1}$ in TOP-$PbI_2$ sample, indicative of a new binding formation between TOP and $PbI_2$, and

thus the $PbI_2$ adduct.[61] The new binding interaction in TOP-$PbI_2$ can arise from P-Pb or P-I but the latter can be possibly ruled out because dissolving the elemental iodine in TOP (*i.e.*, the sample of TOP-$I_2$) does not induce such an absorption in that range (Figure 3a, purple line). We also gathered the initial XRD information on the proposed TOP·$PbI_2$ adduct shown in Figure S9, which reveal a completely different crystal structure from that of the free parent $PbI_2$. Such a XRD change was also observed in the case of DMSO·$PbI_2$ adduct (Figure S9).

To further investigate the interactions between TOP and $PbI_2$, we then carried out nuclear magnetic resonance (NMR) measurement. Figure 3b shows the $^{31}P$ NMR spectra of the free TOP and TOP-$PbI_2$ precursor solution with different $PbI_2$ concentrations. It is seen that the narrow characteristic peak of the free TOP at -32.0 ppm broadens and diminishes in intensity and moves downfield with the increase of the $PbI_2$ content in TOP, which is also followed by the appearance of a sharp peak at ~55 ppm. Based on a comparison to the case of TOP=O and TOP-Se, the two common compound states of TOP, which feature resonance positions at 47.4 ppm and 30.0 ppm, respectively, we interpret our observed sharp peak at ~55 ppm as the formation of TOP·$PbI_2$ compound in the precursor solution. As for the broadening and shifting of the signal peak at -32.0 ppm, it can be due to the coordination effect of TOP solvent with $PbI_2$, which helps to stabilize the formed TOP·$PbI_2$ compound.

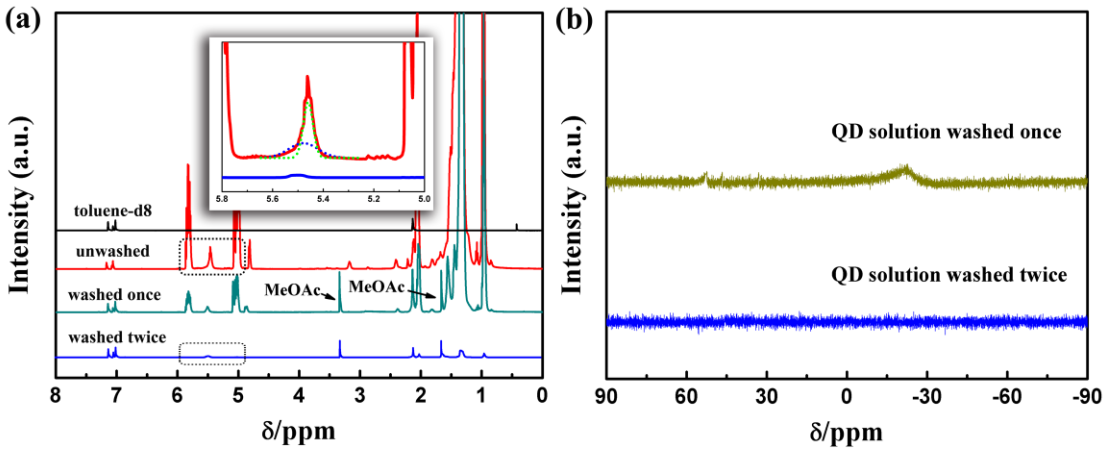


**Figure 4.** (a) $^1H$ NMR spectra of the TOP-QD solutions that are unwashed, washed once, and washed twice with MeOAc (both are dispersed in Toluene-d8 with

concentration of ~$10^{-3}$ mol/L). Inset in (a) is the blown-up of the characteristic signal change between unwashed and washed samples. (b) $^{31}$P NMR spectra of a TOP-QD Toluene-d8 solution after once- and twice-washing with MeOAc.

Next, to clearly identify the possible ligands on surface of the TOP-QDs, we then carried out $^{1}$H NMR measurement. NMR spectroscopy is the most powerful and commonly employed method of identifying ligands on surface of the colloidal QDs. Within a NMR spectrum, ligands bound to the surface of the QDs can be distinguished from those in solution through their chemical shift or line width.[62] In Figure 4a, focusing on the alkene resonance signal region around 5.4~5.5 ppm, we found that the unwashed QD solution features a broadened resonance peak with a slight shift to higher ppm values when compared to the neat oleic acid and oleylamine (5.42 ppm) (All reference $^{1}$H NMR spectra of the free MeOAc, oleic acid, oleylamine, TOP, and ODE are presented in Figure S10). In fact, this signal feature has been attributed to the oleylammonium oleate ligands (a product formed by deprotonation reaction between oleic acid and oleylamine) dynamically interacting with the QD surface.[12, 15] Further, this broadened signal peak can be deconvoluted into two well-resolved contributions, one is detected at 5.47 ppm, which features weaker and broadened, it can be thus attributed to result from the bound ligands of oleylammonium oleate. The other peak is located at 5.42 ppm, which is sharp and can be assigned to the free oleic acid and/or oleylamine. This assignment is further supported by the observation in spectra of a once-washed sample, in which sharp peak located at 5.42 ppm was greatly reduced while the weak contribution at 5.47 ppm was almost unchanged. More significantly, after second washing with MeOAc, those residual organics such as ODE and unbound OA/m have been almost completely removed, yet the broad resonance component at 5.47 ppm still remains, suggesting tightly bound oleylammonium oleate ligand on surface of the QDs. The successful conservation of these protective organic ligands even after twice anti-solvent washing thus explains the excellent colloidal stability of the obtained TOP-QDs. However, we

also note that three times of MeOAc washing will completely strip the ligands from QDs and eventually cause aggregation of the QDs as shown in Figure S1. Additionally, it is important to stress that although our synthetic route involves using TOP in the preparation of the precursor of $PbI_2$, but the resulting purified QD solution does not contain any detectable P signal as shown in Figure 4b. Therefore, we conclude that only alkylammonium oleate serves as the binding ligand on TOP-QD surface. Also, from the above results, we infer that in our preparation route TOP serves as a critical coordinating solvent that dissolves $PbI_2$ powder and thus forming highly reactive intermediate precursor, which accelerates nucleation and growth of the nanocrystals and yields $CsPbI_3$ QDs with improved crystalline quality.

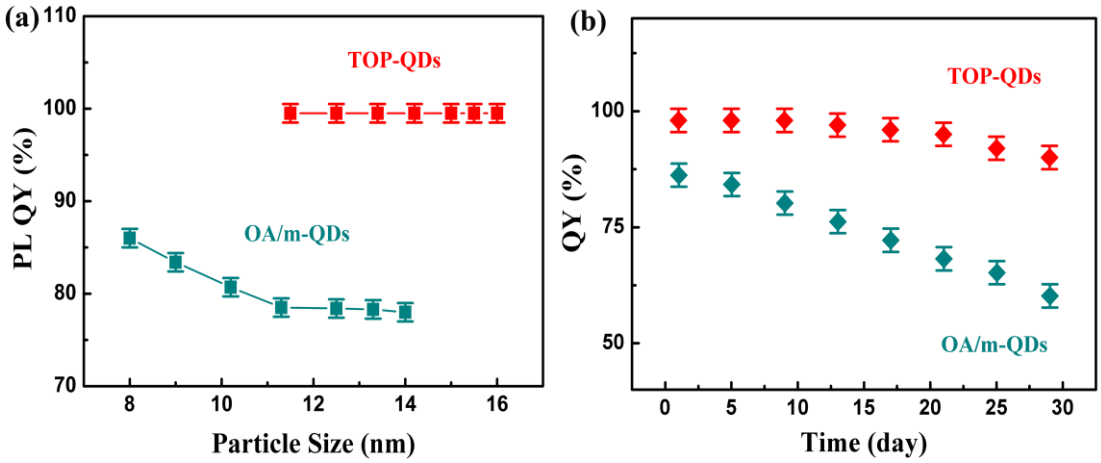


**Figure 5.** (a) Dependence of the PL QYs of the OA/m-QDs and TOP-QDs on their particle size. (b) Change of the PL QY of the OA/m-, TOP-$CsPbI_3$ QDs *versus* storage time, where QD solutions synthesized at 140 °C were stored in a sealed bottle under ambient conditions. All QD samples were washed twice with MeOAc before QY measurement.

Photophysical properties of the resulting $CsPbI_3$ QDs were evaluated by measuring their PL QYs using a commercial Hamamatsu setup (see details in Methods section). The absolute QY was defined by the following equation, $QY = N_{emit}/N_{absorb}$, where $N_{emit}$ and $N_{absorb}$ are numbers of emitted and absorbed photons, respectively. Very

encouragingly, twice-washed QDs in all sizes prepared from TOP route exhibit the best-so-far QYs of up to near 100%, higher than that of the OA/m route-produced ones with 78-84% as summarized in Figure 5a. This behavior, indicative of the absence of non-radiative pathways within the TOP-QDs, is very unusual and rarely observed, even in those traditional high-quality QDs such as $CuInS_2$ and CdS/Se QDs employing those advanced core/shell passivation techniques.[63-67] Note that the measured QY values for the reference OA/m-$CsPbI_3$ QDs are comparable to that of the previously reported literature values.[9] The achieved near 100% PL QYs of the TOP-QDs along with their narrow emission line widths observed in Figure 1c thus suggest the almost complete elimination of the non-radiative defects in TOP-$CsPbI_3$ QDs, which are normally an intrinsic consequence of the nanometer-sized particles. This remarkable property of the TOP-QDs renders them superior for use in fluorescence devices and excitonic solar cells.[68] In addition, it is worth mentioning that in standard OA/m route, a general decrease in QYs was found when increasing the size of the QDs as shown in Figure 5a, which means that the non-radiative recombination due to the trapping defects has larger influence with the size increasing. However, in our case, QYs remain constant even the size of the TOP-QDs reached about 16 nm (Figure 5a). Interestingly, we found that lowering the concentration of $PbI_2$ in TOP to 0.5 mol/L and synthesized at 130 °C can also yield TOP-QDs with high QYs of ~100%. But similar to the typical trend in OA/m route, at this given concentration of $PbI_2$, QYs decrease as the increase of TOP-QD size (drop from ~100% of 11 nm to ~85% of 16 nm), highlighting the importance of Pb-rich conditions for achieving high-quality large-sized $CsPbI_3$ QDs. More research work is needed to further investigate the influence of the reagent stoichiometric ratio on photophysical properties of the TOP-QDs.

In order to show the retention of these resulting TOP-QDs in solution and evaluate their photochemical stability, we conducted the aging of a twice-washed QD colloidal solution by recording its QY. First, $^1$H NMR spectra shown in Figure 4a confirm that after twice MeOAc washing those remaining organics including ODE and unbound

ligands are almost completely removed from QD solution, given that the strong resonance signals assignable to these organics can not be observed. Figure 5b shows that after twice MeOAc washing, TOP-$CsPbI_3$ QDs synthesized at 140 °C yield stable high QY of 100% for the first 9 days and retain ~85% of its initial value after storage for 1 month. In contrast, OA/m-QDs show a decreased QY from the initial 86% to 60% after 30 days storage, which in turn suggests a better chemical stability of the resulting TOP-QDs. The excellent chemical stability of the resulting TOP-QDs is considered to result from their improved crystalline quality as revealed by the observation of smaller Stokes shifts and lower Urbach energies, which alleviates the formation of quenching defects within QDs. The slightly decreased QY of TOP-QDs over time is presumably attributed to the loss of part of the surface ligands, which leaves the QDs incompletely passivated and leads to the presence of trapping defects.

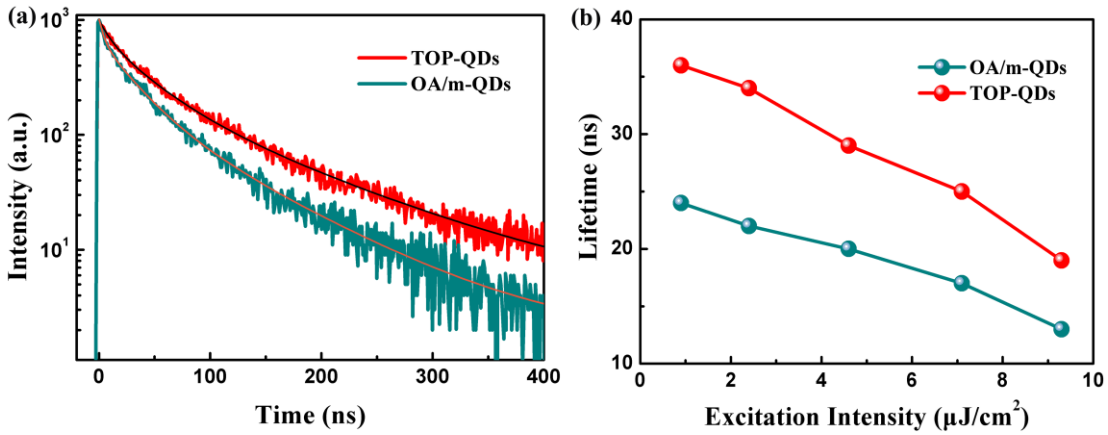


**Figure 6.** (a) Time-resolved PL decay curves of the OA/m- and TOP-QDs (normalized to the initial PL intensity) with excitation intensity and wavelength of 0.9 $\mu$J/cm$^2$ and 532 nm, respectively. (b) Excitation intensity dependence of the PL decay effective lifetimes for OA/m- and TOP-QDs.

To understand the outstanding photophysical properties of the resulting TOP-$CsPbI_3$ QDs, we then carried out PL decay measurements on both solution-dispersed samples. Figure 6a gives the typical time-resolved normalized PL decays for OA/m-QDs (~80% QY) and TOP-QDs (~100% QY) with similar particle

size and PL emission peak position (~685 nm), where the pump light wavelength is 532 nm and the excitation intensity is 0.9 $\mu$J/cm$^2$. It is clearly observed that the PL kinetics of the TOP-QDs is slower than that of OA/m-QDs. According to the definition of PL lifetime $t_{1/e}$, $I_{PL}(t_{1/e}) = I_{PL}(0)/e$,[69] where $I_{PL}(t)$ represents the PL decay dynamics, we obtained the effective PL lifetime of ~22 ns and 36 ns for OA/m-QDs and TOP-QDs, respectively. It is known that the exciton binding energy ($E_b$) in QDs is much larger than that of their bulk counterparts. For example, $E_b$ of the $CH_3NH_3PbBr_3$ QDs is about 375 meV, while $E_b$ of the bulk $CH_3NH_3PbBr_3$ is about 40-65 meV.[9, 47, 70, 71] Then, the $E_b$ of $CsPbI_3$ QDs can be also expected much larger than that of the bulk counterpart (~20 meV).[9, 47, 70] Therefore, the PL emission can be considered to originate from radiative relaxation of excitons in the $CsPbI_3$ QDs.[72, 73]

It is well known that in addition to the intrinsic properties of the semiconductors, surface chemistry and passivation of the QDs would have a great influence on their exciton lifetimes, *i.e.*, if the QD surface is not well passivated, surface defects will exist, which in turn give rise to the non-radiative surface states and lead to shorter exciton lifetimes.[11, 23, 58] It is found that the effective PL lifetime obtained for OA/m-QDs is consistent with previous reports,[9, 74] but the lifetime for TOP-QDs increases largely, implying that our TOP-based synthetic route successfully suppresses the formation of non-radiative recombination pathways on surface of the $CsPbI_3$ QDs. This finding is also in good agreement with the high QYs obtained in TOP-QDs.

Dependence of the PL kinetics on excitation intensity is shown in Figure S11. Figure 6b summarizes the dependence of the effective PL lifetime on the excitation intensity. For all of the excitation intensities, we see a substantial increase in lifetime of the TOP-QDs as compared to those of OA/m-QDs, which can be understood by the above discussion. In addition, for both kinds of QDs, the average PL lifetimes decreased as the increase of excitation intensity. This phenomenon can be expected to result from two-body recombination (*i.e.*, radiative electron and hole recombination) and/or three-body recombination processes (*i.e.*, Auger recombination) in both QDs, which typically cause a reduction in PL lifetimes.[69, 75, 76]

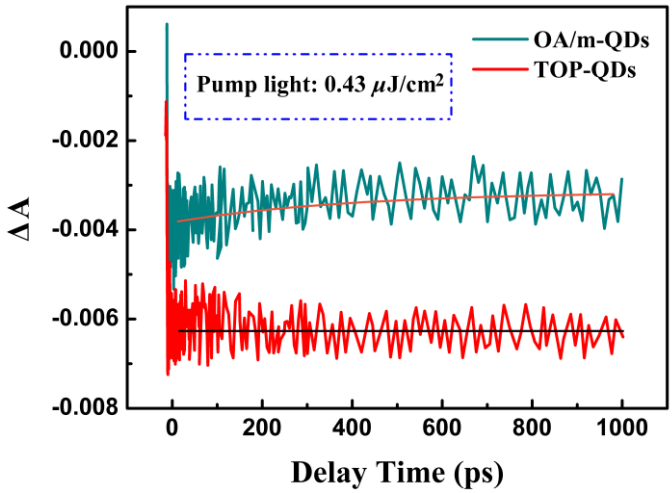


**Figure 7.** TA response of the TOP- and OA/m-QDs measured with a pump light wavelength of 470 nm and probe light wavelengths of 670 and 650 nm for TOP-QDs and OA/m-QDs, respectively. The probe light wavelength is determined by their own maximum exciton bleach. Pump light intensity: 0.43 $\mu$J/cm$^2$.

In order to gain more insight into the fundamental physics behind these appealing optical properties, we therefore monitored the ultrafast exciton relaxation dynamics through TA spectrum measurements. Figure S12 shows the TA spectra measured with a pump light intensity of 0.43 $\mu$J/cm$^2$, in which bleach signals with peaks at 670 and 650 nm can be observed for TOP-QDs and OA/m-QDs, respectively, corresponding to the optical absorbance change (ΔA) between the LUMO and HOMO in the $CsPbI_3$ QDs. In this case, it is known that the ΔA is proportional to the exciton density $n$ at the lowest excited states in the QDs.[77] Figure S13 shows the normalized TA decays of TOP-QDs and OA/m-QDs at different pump excitation intensities with probing wavelengths of 670 nm and 650 nm, respectively. For both kinds of QDs, fast decay processes appear in their TA responses when the pump intensity is larger than 0.8 $\mu$J/cm$^2$, and the TA responses decay faster as the pump intensity increases further. This phenomenon indicates the occurrence of three-body Auger recombination processes in both $CsPbI_3$ QDs under the large pump intensity excitation.[77-79] However, when the pump intensity is smaller than 0.8 $\mu$J/cm$^2$, we found that the fast decay

process disappeared and the waveforms of the TA responses overlapped with each other very well when they were normalized at the peak intensity. This result indicates that three-body recombination is negligible under such low pump intensity excitation, and only one-body and two-body recombination processes can be observed here. Figure 7a shows TA responses of TOP- and OA/m-QDs measured with a low pump light intensity of 0.43 $\mu$J/cm$^2$. It is seen that the exciton bleach signal of OA/m-QD sample shows a slow single-exponential decay with a background signal $y_0$, while that of TOP-QDs is not changed in 1ns time scale. Fitting the TA response of OA/m-QDs to the following equation (2) gives a decay constant $\tau$ of 400 ± 30 ps ($A_0/(A_0+y_0)$: 15%). As discussed above, this result means that about 15% of the photo-excited excitons recombine through the non-radiative recombination pathway due to defects or surface trap states in OA/m-QDs and ~85% recombine through two-body radiative pathway, which is also consistent with their measured QYs of ~80%.

$$\mathrm{Y}(t) = A_0 \exp(\frac{-t}{\tau}) + y_0 \quad (2)$$

However, we couldn't fit the TA curve of TOP-QDs using the same exponential function because no decay can be resolved in the initial 1 ns time scale, which in turn suggests the negligible electron or hole trapping pathways in these TOP-QDs.

## Conclusions

In conclusion, we have presented a reproducible TOP-based route which yields phase-stable monodisperse $CsPbI_3$ QDs with the best-so-far quantum efficiency up to 100%. Time-resolved PL decays indicate longer radiative lifetimes in the resulting QDs compared to the previous ones. Ultrafast TA spectroscopy measurements confirm the negligible electron or hole trapping pathways in TOP-$CsPbI_3$ QDs, which thus reveal the fundamental physics behind these superior properties. Another encouraging result employing TOP route is the enhanced chemical stability of the $CsPbI_3$ QDs, which used to be the main problem preventing these amazing nanoparticles from

being further studied. The successful synthesis of the phase-stable $CsPbI_3$ QDs with near-perfect photophysical properties not only benefits fundamental research in the field of nanocrystals but also significantly broadens the possibilities of using perovskite QDs for a wide range of practical applications.

## Methods

### Synthesis of TOP-$CsPbI_3$ QDs

All chemicals were used as received without further purification. 0.92 g of $PbI_2$ powder (98%, Kanto Chemicals, Japan, pre-dried at 60 °C under vacuum for overnight) was added to 2.5 mL of tri-n-octylphosphine (TOP, 90%, Aldrich) to prepare a 0.8 M TOP-$PbI_2$ stock solution. The mixture was vigorously stirred on a hot plate for a sufficiently long time at 90-100 °C, usually one week (**NOTE:** using the other purity of TOP (*e.g.*, 97%) would require a longer time, usually 8-10 days). Prior to use, TOP-$PbI_2$ stock solution was centrifuged at 4,000 rpm for 3 min to remove any excess salts. A mixture of 0.12 g of $Cs_2CO_3$ (99.9%, Aldrich), 0.4 mL of oleic acid (OA, ≥ 65.0%, Wako Pure Chemicals, Japan), 0.4 mL of oleylamine (OAm, technical grade, 70%, Aldrich), and 12 mL of octadecene (ODE, technical grade, 90%, Aldrich) was loaded into a 50 mL three-neck flask and degassed at 110 °C for 3 h with stirring (temperature was monitored using a Sanyo mercury thermometer, Japan). It was then heated to 120 °C under nitrogen atmosphere until the solution became clear. The temperature was then set from 100 to 170 °C depending on the desired QD size for the subsequent quick injection of the prepared TOP-$PbI_2$ solution. About 5 secs after injection, the reaction was quenched by immediate immersion of the flask into an ice bath, after which an equivalent volume of methyl acetate (MeOAc, anhydrous 99.5%, Aldrich) was added to precipitate the QDs followed by centrifugation at 4,000 rpm for 3 min. The supernatant was discarded and the precipitate was dispersed in hexane. It was then re-centrifuged at 4,000 rpm for 3 min to remove large particles and remaining impurities. The above procedure can be repeated twice for obtaining more purified QD solutions (three times of washing will completely strip the ligands from QDs and eventually cause aggregation of the QDs as shown in Figure S1). It is noted

that for $CsPbI_3$ QDs synthesized below 130 °C, a certain amount of yellow by-products could be observed after hexane dispersion. In this case, QDs can still be collected by centrifugation at 4,000 rpm for 2 min. For smaller $CsPbI_3$ QDs synthesized below 120 °C, purification of the QDs was carried out by first mixing the crude solution with hexane (v/v, 1:6), the mixture was then cooled in a freezer at minus 20 °C for 3 h and taken out, centrifuged at 4,000 rpm for 1 min. After centrifugation, the precipitate was discarded and the supernatant was collected. The above procedure can be repeated several times for obtaining more purified QD solutions. The resulting colloidal QD solutions were kept in the dark at 4 °C and centrifuged before use.

**Synthesis of OA/m-$CsPbI_3$ QDs (Reference 9)**

**Preparation of Cs-oleate**: 0.814 g of $Cs_2CO_3$ was loaded into 100 mL three-neck flask along with 40 mL of ODE and 2.5 mL of OA, dried for 1h at 120 ºC, and then heated under nitrogen to 130 ºC until all $Cs_2CO_3$ reacted with OA. It has to be preheated to 100 ºC before injection since Cs-oleate precipitates out of ODE at room-temperature.

**OA/m-$CsPbI_3$ QD Synthesis**: 10 mL of ODE and 0.17 g of $PbI_2$ were loaded into 50 mL three-neck flask and dried under vacuum for 1h at 120 ºC. OA and OAm (1 mL each) were injected at 120 ºC under $N_2$. After complete solubilization of $PbI_2$, the temperature was adjusted to 100-180 ºC and Cs-oleate solution (0.8 mL, 0.125 M in ODE, prepared as described above) was quickly injected. About 5 secs later, the reaction mixture was cooled by the ice-water bath. Purification process was finished as described above for the TOP-$CsPbI_3$ QDs.

**Characterization**

The phase identification was carried out using a powder X-ray diffraction (XRD, TTR-III, Rigaku Corp., Japan). The morphology and crystal structure of the prepared samples were characterized using a high-resolution transmission electron microscopy (HRTEM, JEM-2100F, Japan). X-ray photoelectron spectroscopy (XPS) data were accumulated on a photoelectron spectrometer, JPS-90MX (JEOL, Ltd., Japan). UV-vis

absorption spectra were recorded with a spectrophotometer (HITACHI, U-3900H, Japan). Fluorescence emission spectra were recorded on a FP-6500 spectrophotometer (JASCO, Japan). Solution nuclear magnetic resonance (NMR) spectra ($^{1}$H and $^{31}$P) were recorded with a JEOL ECA-500 (500 MHz) (Japan) instrument, 25 °C. Fourier transform-infrared spectra (FT-IR) were recorded using a Nicolet 6700 FT-IR spectrophotometer equipment. The absolute fluorescence quantum yield of the QD solutions was measured by using an integrating sphere on an Absolute PL Quantum Yield Spectrometer C11347 at an excitation power of 0.1 mW (Hamamatsu, Japan). PL decay was measured using a NIR PL lifetime spectrometer (C12132, Hamamatsu Photonics). Transient absorption (TA) measurements were performed using a fs TA setup. The laser source was a titanium/sapphire laser (CPA-2010, Clark-MXR Inc.) with a wavelength of 775 nm, a repetition rate of 1KHz, and a pulse width of 150 fs. The light was separated into two parts. One part was incident on a sapphire plate to generate white light for the probe beam. The other part was used to pump an optical parametric amplifier (OPA) (a TOAPS from Quantronix) to generate light pulses with a wavelength tunable from 290 nm to 3 $\mu$m. It was used as a pump light to excite the sample.[78-80] In this study, a pump light with a wavelength of 470 nm was used to excite the QDs. The pump light intensity was changed from 0.43 $\mu$J/cm$^2$ to 142 $\mu$J/cm$^2$. Time-resolved TA spectra from 530 nm to 750 nm were obtained with a temporal resolution of 100 fs.

## Associated content

### Supporting Information

QD washing procedures, additional HRTEM images, XPS spectra, UV-vis absorption spectra, XRD patterns, photographs of $CsPbI_3$ QD solutions, NMR spectra, PL decays, and TA responses. This material is available free of charge *via* the Internet at http://pubs.acs.org.

## Author information

### Corresponding Author

shen@pc.uec.ac.jp

**Notes**

The authors declare no competing financial interest.

## Acknowledgements

This research was supported by the Japan Science and Technology Agency (JST) CREST program, JST PRESTO program, the MEXT KAKENHI Grant (Grant Number 26286013, 17H02736) and the UEC postdoctoral program.

## References

1. Swarnkar, A.; Marshall, A. R.; Sanehira, E. M.; Chernomordik, B. D.; Moore, D. T.; Christians, J. A.; Chakrabarti, T.; Luther, J. M. Quantum Dot-Induced Phase Stabilization of Alpha-CsPbI3 Perovskite for High-Efficiency Photovoltaics. *Science* **2016**, 354, 92-95.

2. Song, J. Z.; Li, J. H.; Li, X. M.; Xu, L. M.; Dong, Y. H.; Zeng, H. B. Quantum Dot Light-Emitting Diodes Based on Inorganic Perovskite Cesium Lead Halides (CsPbX3). *Adv. Mater.* **2015**, 27, 7162-7167.

3. Ramasamy, P.; Lim, D. H.; Kim, B.; Lee, S. H.; Lee, M. S.; Lee, J. S. All-Inorganic Cesium Lead Halide Perovskite Nanocrystals for Photodetector Applications. *Chem. Commun.* **2016**, 52, 2067-2070.

4. Sutherland, B. R.; Sargent, E. H. Perovskite Photonic Sources. *Nat. Photonics* **2016**, 10, 295-302.

5. Liu, H.; Wu, Z.; Shao, J.; Yao, D.; Gao, H.; Liu, Y.; Yu, W.; Zhang, H.; Yang, B. CsPbxMn1–xCl3 Perovskite Quantum Dots with High Mn Substitution Ratio. *ACS Nano* **2017**, 2, 2239-2247.

6. Ma, Q. S.; Huang, S. J.; Wen, X. M.; Green, M. A.; Ho-Baillie, A. W. Y. Hole Transport Layer Free Inorganic CsPbIBr2 Perovskite Solar Cell by Dual Source Thermal Evaporation. *Adv. Energy Mater.* **2016**, 6, 1502202.

7. Yantara, N.; Bhaumik, S.; Yan, F.; Sabba, D.; Dewi, H. A.; Mathews, N.; Boix, P. P.; Demir, H. V.; Mhaisalkar, S. Inorganic Halide Perovskites for Efficient

Light-Emitting Diodes. *J. Phys. Chem. Lett.* **2015**, 6, 4360-4364.

8. Butkus, J.; Vashishtha, P.; Chen, K.; Gallaher, J. K.; Prasad, S. K. K.; Metin, D. Z.; Laufersky, G.; Gaston, N.; Halpert, J. E.; Hodgkiss, J. M. The Evolution of Quantum Confinement in CsPbBr3 Perovskite Nanocrystals. *Chem. Mater.* **2017**, 29, 3644-3652.

9. Protesescu, L.; Yakunin, S.; Bodnarchuk, M. I.; Krieg, F.; Caputo, R.; Hendon, C. H.; Yang, R. X.; Walsh, A.; Kovalenko, M. V. Nanocrystals of Cesium Lead Halide Perovskites (CsPbX3, X = Cl, Br, and I): Novel Optoelectronic Materials Showing Bright Emission with Wide Color Gamut. *Nano Lett.* **2015**, 15, 3692-3696.

10. Yettapu, G. R.; Talukdar, D.; Sarkar, S.; Swarnkar, A.; Nag, A.; Ghosh, P.; Mandal, P. Terahertz Conductivity within Colloidal CsPbBr3 Perovskite Nanocrystals: Remarkably High Carrier Mobilities and Large Diffusion Lengths. *Nano Lett.* **2016**, 16, 4838-4848.

11. Wu, K. F.; Liang, G. J.; Shane, Q. Y.; Ren, Y. P.; Kong, D. G.; Lian, T. Q. Ultrafast Interfacial Electron and Hole Transfer from CsPbBr3 Perovskite Quantum Dots. *J. Am. Chem. Soc.* **2015**, 137, 12792-12795.

12. De Roo, J.; Ibanez, M.; Geiregat, P.; Nedelcu, G.; Walravens, W.; Maes, J.; Martins, J. C.; Van Driessche, I.; Koyalenko, M. V.; Hens, Z. Highly Dynamic Ligand Binding and Light Absorption Coefficient of Cesium Lead Bromide Perovskite Nanocrystals. *ACS Nano* **2016**, 10, 2071-2081.

13. Eperon, G. E.; Paterno, G. M.; Sutton, R. J.; Zampetti, A.; Haghighirad, A. A.; Cacialli, F.; Snaith, H. J. Inorganic Caesium Lead Iodide Perovskite Solar Cells. *J. Mater. Chem. A* **2015**, 3, 19688-19695.

14. Palazon, F.; Almeida, G.; Akkerman, Q. A.; De Trizio, L.; Dang, Z.; Prato, M.; Manna, L. Changing the Dimensionality of Cesium Lead Bromide Nanocrystals by Reversible Postsynthesis Transformations with Amines. *Chem. Mater* **2017**, 29, 4167-4171.

15. Pan, A. Z.; He, B.; Fan, X. Y.; Liu, Z. K.; Urban, J. J.; Alivisatos, A. P.; He, L.; Liu, Y. Insight into the Ligand-Mediated Synthesis of Colloidal CsPbBr3 Perovskite

Nanocrystals: The Role of Organic Acid, Base, and Cesium Precursors. *ACS Nano* **2016**, 10, 7943-7954.

16. Ip, A. H.; Kiani, A.; Kramer, I. J.; Voznyy, O.; Movahed, H. F.; Levina, L.; Adachi, M. M.; Hoogland, S.; Sargent, E. H. Infrared Colloidal Quantum Dot Photovoltaics via Coupling Enhancement and Agglomeration Suppression. *ACS Nano* **2015**, 9, 8833-8842.

17. Carey, G. H.; Abdelhady, A. L.; Ning, Z. J.; Thon, S. M.; Bakr, O. M.; Sargent, E. H. Colloidal Quantum Dot Solar Cells. *Chem. Rev.* **2015**, 115, 12732-12763.

18. Barkhouse, D. A. R.; Pattantyus-Abraham, A. G.; Levina, L.; Sargent, E. H. Thiols Passivate Recombination Centers in Colloidal Quantum Dots Leading to Enhanced Photovoltaic Device Efficiency. *ACS Nano* **2008**, 2, 2356-2362.

19. Pan, Z. X.; Mora-Sero, I.; Shen, Q.; Zhang, H.; Li, Y.; Zhao, K.; Wang, J.; Zhong, X. H.; Bisquert, J. High-Efficiency "Green" Quantum Dot Solar Cells. *J. Am. Chem. Soc.* **2014**, 136, 9203-9210.

20. Burroughes, J. H.; Bradley, D. D. C.; Brown, A. R.; Marks, R. N.; Mackay, K.; Friend, R. H.; Burn, P. L.; Holmes, A. B. Light-Emitting-Diodes Based on Conjugated Polymers. *Nature* **1990**, 347, 539-541.

21. Shirasaki, Y.; Supran, G. J.; Bawendi, M. G.; Bulovic, V. Emergence of Colloidal Quantum-Dot Light-Emitting Technologies. *Nat. Photonics* **2013**, 7, 13-23.

22. Zhang, X. Y.; Sun, C.; Zhang, Y.; Wu, H.; Ji, C. Y.; Chuai, Y. H.; Wang, P.; Wen, S. P.; Zhang, C. F.; Yu, W. W. Bright Perovskite Nanocrystal Films for Efficient Light-Emitting Devices. *J. Phys. Chem. Lett.* **2016**, 7, 4602-4610.

23. Li, J.; Xu, L.; Wang, T.; Song, J.; Chen, J.; Xue, J.; Dong, Y.; Cai, B.; Shan, Q.; Han, B. 50-Fold EQE Improvement up to 6.27% of Solution-Processed All-Inorganic Perovskite CsPbBr3 QLEDs via Surface Ligand Density Control. *Adv. Mater.* **2017**, 29, 1603885.

24. Yin, Y.; Alivisatos, A. P. Colloidal Nanocrystal Synthesis and the Organic-Inorganic Interface. *Nature* **2005**, 437, 664-670.

25. Gao, Y.; Peng, X. G. Photogenerated Excitons in Plain Core CdSe Nanocrystals

with Unity Radiative Decay in Single Channel: The Effects of Surface and Ligands. *J. Am. Chem. Soc.* **2015**, 137, 4230-4235.

26. Zhang, F.; Huang, S.; Wang, P.; Chen, X. M.; Zhao, S. L.; Dong, Y. P.; Zhong, H. Z. Colloidal Synthesis of Air-Stable CH3NH3PbI3 Quantum Dots by Gaining Chemical Insight into the Solvent Effects. *Chem. Mater.* **2017**, 29, 3793-3799.

27. Harrell, S. M.; McBride, J. R.; Rosenthal, S. J. Synthesis of Ultrasmall and Magic-Sized CdSe Nanocrystals. *Chem. Mater.* **2013**, 25, 1199-1210.

28. Murray, C. B.; Norris, D. J.; Bawendi, M. G. Synthesis and Characterization of Nearly Monodisperse Cde (E = S, Se, Te) Semiconductor Nanocrystallites. *J. Am. Chem. Soc.* **1993**, 115, 8706-8715.

29. Steckel, J. S.; Yen, B. K. H.; Oertel, D. C.; Bawendi, M. G. On the Mechanism of Lead Chalcogenide Nanocrystal Formation. *J. Am. Chem. Soc.* **2006**, 128, 13032-13033.

30. Micic, O. I.; Cheong, H. M.; Fu, H.; Zunger, A.; Sprague, J. R.; Mascarenhas, A.; Nozik, A. J. Size-Dependent Spectroscopy of InP Quantum Dots. *J. Phys. Chem. B* **1997**, 101, 4904-4912.

31. Sun, L. F.; Bao, L.; Hyun, B. R.; Bartnik, A. C.; Zhong, Y. W.; Reed, J. C.; Pang, D. W.; Abruna, H. D.; Malliaras, G. G.; Wise, F. W. Electrogenerated Chemiluminescence from PbS Quantum Dots. *Nano Lett.* **2009**, 9, 789-793.

32. Talapin, D. V.; Rogach, A. L.; Kornowski, A.; Haase, M.; Weller, H. Highly Luminescent Monodisperse CdSe and CdSe/ZnS Nanocrystals Synthesized in a Hexadecylamine-Trioctylphosphine Oxide-Trioctylphospine Mixture. *Nano Lett.* **2001**, 1, 207-211.

33. Yu, K.; Zaman, B.; Singh, S.; Wang, D. S.; Ripmeester, J. A. The Effect of Dispersion Media on Photoluminescence of Colloidal CdSe Nanocrystals Synthesized From TOP. *Chem. Mater.* **2005**, 17, 2552-2561.

34. Liu, H. T.; Owen, J. S.; Alivisatos, A. P. Mechanistic Study of Precursor Evolution in Colloidal Group II-VI Semiconductor Nanocrystal Synthesis. *J. Am. Chem. Soc.* **2007**, 129, 305-312.

35. Jang, K.; Lee, I. Y.; Xu, J.; Choi, J.; Jin, J.; Park, J. H.; Kim, H. J.; Kim, G. H.; Son, S. U. Colloidal Synthesis of SnSe Nanocolumns through Tin Precursor Chemistry and Their Optoelectrical Properties. *Crystal Growth & Design* **2012**, 12, 3388-3391.

36. Green, M. The Nature of Quantum Dot Capping Ligands. *J. Mater. Chem.* **2010**, 20, 5797-5809.

37. Becerra, L. R.; Murray, C. B.; Griffin, R. G.; Bawendi, M. G. Investigation of the Surface-Morphology of Capped Cdse Nanocrystallites by P-31 Nuclear-Magnetic-Resonance. *J. Chem. Phys.* **1994**, 100, 3297-3300.

38. Jellicoe, T. C.; Richter, J. M.; Glass, H. F. J.; Tabachnyk, M.; Brady, R.; Dutton, S. E.; Rao, A.; Friend, R. H.; Credgington, D.; Greenham, N. C.; Bohm, M. L. Synthesis and Optical Properties of Lead-Free Cesium Tin Halide Perovskite Nanocrystals. *J. Am. Chem. Soc.* **2016**, 138, 2941-2944.

39. Hassan, Y.; Song, Y.; Pensack, R. D.; Abdelrahman, A. I.; Kobayashi, Y.; Winnik, M. A.; Scholes, G. D. Structure-Tuned Lead Halide Perovskite Nanocrystals. *Adv. Mater.* **2016**, 28, 566-573.

40. Sun, S. B.; Yuan, D.; Xu, Y.; Wang, A. F.; Deng, Z. T. Ligand-Mediated Synthesis of Shape-Controlled Cesium Lead Halide Perovskite Nanocrystals via Reprecipitation Process at Room Temperature. *ACS Nano* **2016**, 10, 3648-3657.

41. Chastain, J.; King, R. C.; Moulder, J. *Handbook of X-ray Photoelectron Spectroscopy: A Reference Book of Standard Spectra for Identification and Interpretation of XPS Data*. Physical Electronics Eden Prairie, MN: 1995.

42. Morgan, W. E.; Van Wazer, J. R.; Stec, W. J. Inner-Orbital Photoelectron Spectroscopy of the Alkali Metal Halides, Perchlorates, Phosphates, and Pyrophosphates. *J. Am. Chem. Soc.* **1973**, 95, 751-755.

43. Hoffman, J. B.; Schleper, A. L.; Kamat, P. V. Transformation of Sintered CsPbBr3 Nanocrystals to Cubic CsPbI3 and Gradient CsPbBrxI3-x through Halide Exchange. *J. Am. Chem. Soc.* **2016**, 138, 8603-8611.

44. Chang, Y. H.; Park, C. H.; Matsuishi, K. First-Principles Study of the Structural

and the Electronic Properties of the Lead-Halide-Based Inorganic-Organic Perovskites (CH3NH3)PbX3 and CsPbX3 (X = Cl, Br, I). *J. Korean Phys. Soc.* **2004**, 44, 889-893.

45. Koolyk, M.; Amgar, D.; Aharon, S.; Etgar, L. Kinetics of Cesium Lead Halide Perovskite Nanoparticle Growth; Focusing and De-focusing of Size Distribution. *Nanoscale* **2016**, 8, 6403-6409.

46. Murtaza, G.; Ahmad, I. First Principle Study of the Structural and Optoelectronic Properties of Cubic Perovskites CsPbM3 (M=Cl, Br, I). *Physica B* **2011**, 406, 3222-3229.

47. Zhang, F.; Zhong, H. Z.; Chen, C.; Wu, X. G.; Hu, X. M.; Huang, H. L.; Han, J. B.; Zou, B. S.; Dong, Y. P. Brightly Luminescent and Color-Tunable Colloidal CH3NH3PbX3 (X = Br, I, Cl) Quantum Dots: Potential Alternatives for Display Technology. *ACS Nano* **2015**, 9, 4533-4542.

48. Du, H.; Chen, C. L.; Krishnan, R.; Krauss, T. D.; Harbold, J. M.; Wise, F. W.; Thomas, M. G.; Silcox, J. Optical Properties of Colloidal PbSe Nanocrystals. *Nano Lett.* **2002**, 2, 1321-1324.

49. Boles, M. A.; Ling, D.; Hyeon, T.; Talapin, D. V. The Surface Science of Nanocrystals. *Nat. Mater.* **2016**, 15, 141-153.

50. Urbach, F. The Long-Wavelength Edge of Photographic Sensitivity and of the Electronic Absorption of Solids. *Phys. Rev.* **1953**, 92, 1324.

51. Zhang, W.; Saliba, M.; Moore, D. T.; Pathak, S. K.; Horantner, M. T.; Stergiopoulos, T.; Stranks, S. D.; Eperon, G. E.; Alexander-Webber, J. A.; Abate, A.; Sadhanala, A.; Yao, S. H.; Chen, Y. L.; Friend, R. H.; Estroff, L. A.; Wiesner, U.; Snaith, H. J. Ultrasmooth Organic-Inorganic Perovskite Thin-Film Formation and Crystallization for Efficient Planar Heterojunction Solar Cells. *Nat. Commun.* **2015**, 6, 6142.

52. De Wolf, S.; Holovsky, J.; Moon, S. J.; Loper, P.; Niesen, B.; Ledinsky, M.; Haug, F. J.; Yum, J. H.; Ballif, C. Organometallic Halide Perovskites: Sharp Optical Absorption Edge and Its Relation to Photovoltaic Performance. *J. Phys. Chem. Lett.*

**2014**, 5, 1035-1039.

53. Rai, R. C. Analysis of the Urbach Tails in Absorption Spectra of Undoped ZnO Thin Films. *J. Appl. Phys.* **2013**, 113, 153508.

54. Zhou, J.; Hu, Z.; Zhang, L.; Zhu, Y. Perovskite CsPbBr1.2I1.8 Quantum Dot Alloying for Application in White Light-Emitting Diodes with Excellent Color Rendering Index. *J. Alloys Compd.* **2017**, 708, 517-523.

55. Yuan, L.; Patterson, R.; Wen, X. M.; Zhang, Z. L.; Conibeer, G.; Huang, S. J. Investigation of Anti-Solvent Induced Optical Properties Change of Cesium Lead Bromide Iodide Mixed Perovskite (CsPbBr3-xIx) Quantum Dots. *J. Colloid Interf. Sci.* **2017**, 504, 586-592.

56. Kim, Y.; Yassitepe, E.; Voznyy, O.; Comin, R.; Walters, G.; Gong, X. W.; Kanjanaboos, P.; Nogueira, A. F.; Sargent, E. H. Efficient Luminescence from Perovskite Quantum Dot Solids. *ACS Appl. Mater. Inter.* **2015**, 7, 25007-25013.

57. Liu, F.; Zhu, J.; Wei, J. F.; Li, Y.; Hu, L. H.; Huang, Y.; Takuya, O.; Shen, Q.; Toyoda, T.; Zhang, B.; Yao, J. X.; Dai, S. Y. Ex Situ CdSe Quantum Dot-Sensitized Solar Cells Employing Inorganic Ligand Exchange To Boost Efficiency. *J. Phys. Chem. C* **2014**, 118, 214-222.

58. Tang, J.; Kemp, K. W.; Hoogland, S.; Jeong, K. S.; Liu, H.; Levina, L.; Furukawa, M.; Wang, X. H.; Debnath, R.; Cha, D. K.; Chou, K. W.; Fischer, A.; Amassian, A.; Asbury, J. B.; Sargent, E. H. Colloidal-Quantum-Dot Photovoltaics using Atomic-Ligand Passivation. *Nat. Mater.* **2011**, 10, 765-771.

59. Ahn, N.; Son, D. Y.; Jang, I. H.; Kang, S. M.; Choi, M.; Park, N. G. Highly Reproducible Perovskite Solar Cells with Average Efficiency of 18.3% and Best Efficiency of 19.7% Fabricated via Lewis Base Adduct of Lead(II) Iodide. *J. Am. Chem. Soc.* **2015**, 137, 8696-8699.

60. Chen, W.; Wu, Y. Z.; Yue, Y. F.; Liu, J.; Zhang, W. J.; Yang, X. D.; Chen, H.; Bi, E. B.; Ashraful, I.; Gratzel, M.; Han, L. Y. Efficient and Stable Large-Area Perovskite Solar Cells with Inorganic Charge Extraction Layers. *Science* **2015**, 350, 944-948.

61. Wharf, I.; Gramstad, T.; Makhija, R.; Onyszchuk, M. Synthesis and Vibrational

Spectra of Some Lead (II) Halide Adducts with O-, S-, and N-Donor Atom Ligands. *Can. J. Chem.* **1976**, 54, 3430-3438.

62. Morris-Cohen, A. J.; Malicki, M.; Peterson, M. D.; Slavin, J. W. J.; Weiss, E. A. Chemical, Structural, and Quantitative Analysis of the Ligand Shells of Colloidal Quantum Dots. *Chem. Mater.* **2013**, 25, 1155-1165.

63. Chen, O.; Zhao, J.; Chauhan, V. P.; Cui, J.; Wong, C.; Harris, D. K.; Wei, H.; Han, H. S.; Fukumura, D.; Jain, R. K.; Bawendi, M. G. Compact High-Quality CdSe-CdS Core-Shell Nanocrystals with Narrow Emission Linewidths and Suppressed Blinking. *Nat. Mater* **2013**, 12, 445-451.

64. Christodoulou, S.; Vaccaro, G.; Pinchetti, V.; De Donato, F.; Grim, J. Q.; Casu, A.; Genovese, A.; Vicidomini, G.; Diaspro, A.; Brovelli, S.; Manna, L.; Moreels, I. Synthesis of Highly Luminescent Wurtzite CdSe/CdS Giant-Shell Nanocrystals using a Fast Continuous Injection Route. *J. Mater. Chem. C* **2014**, 2, 3439-3447.

65. Park, J.; Kim, S. W. CuInS2/ZnS Core/Shell Quantum Dots by Cation Exchange and Their Blue-Shifted Photoluminescence. *J. Mater. Chem.* **2011**, 21, 3745-3750.

66. Li, L.; Daou, T. J.; Texier, I.; Tran, T. K. C.; Nguyen, Q. L.; Reiss, P. Highly Luminescent CuInS2/ZnS Core/Shell Nanocrystals: Cadmium-Free Quantum Dots for In Vivo Imaging. *Chem. Mater.* **2009**, 21, 2422-2429.

67. Tyrakowski, C. M.; Shamirian, A.; Rowland, C. E.; Shen, H. Y.; Das, A.; Schaller, R. D.; Snee, P. T. Bright Type II Quantum Dots. *Chem. Mater.* **2015**, 27, 7276-7281.

68. Mora-Sero, I.; Gimenez, S.; Fabregat-Santiago, F.; Gomez, R.; Shen, Q.; Toyoda, T.; Bisquert, J. Recombination in Quantum Dot Sensitized Solar Cells. *Acc. Chem. Res.* **2009**, 42, 1848-1857.

69. Yamada, Y.; Nakamura, T.; Endo, M.; Wakamiya, A.; Kanemitsu, Y. Photocarrier Recombination Dynamics in Perovskite CH3NH3PbI3 for Solar Cell Applications. *J. Am. Chem. Soc.* **2014**, 136, 11610-11613.

70. Zhang, Q.; Su, R.; Liu, X. F.; Xing, J.; Sum, T. C.; Xiong, Q. H. High-Quality Whispering-Gallery-Mode Lasing from Cesium Lead Halide Perovskite Nanoplatelets. *Adv. Funct. Mater.* **2016**, 26, 6238-6245.

71. Yang, Y.; Yang, M. J.; Li, Z.; Crisp, R.; Zhu, K.; Beard, M. C. Comparison of Recombination Dynamics in CH3NH3PbBr3 and CH3NH3PbI3 Perovskite Films: Influence of Exciton Binding Energy. *J. Phys. Chem. Lett.* **2015**, 6, 4688-4692.

72. Swarnkar, A.; Chulliyil, R.; Ravi, V. K.; Irfanullah, M.; Chowdhury, A.; Nag, A. Colloidal CsPbBr3 Perovskite Nanocrystals: Luminescence beyond Traditional Quantum Dots. *Angew. Chem. Int. Edit.* **2015**, 54, 15424-15428.

73. Tong, Y.; Bladt, E.; Ayguler, M. F.; Manzi, A.; Milowska, K. Z.; Hintermayr, V. A.; Docampo, P.; Bals, S.; Urban, A. S.; Polavarapu, L.; Feldmann, J. Highly Luminescent Cesium Lead Halide Perovskite Nanocrystals with Tunable Composition and Thickness by Ultrasonication. *Angew. Chem. Int. Edit.* **2016**, 55, 13887-13892.

74. Ravi, V. K.; Markad, G. B.; Nag, A. Band Edge Energies and Excitonic Transition Probabilities of Colloidal CsPbX3 (X = Cl, Br, I) Perovskite Nanocrystals. *ACS Energy Letters* **2016**, 1, 665-671.

75. Yasuda, H.; Kanemitsu, Y. Dynamics of Nonlinear Blue Photoluminescence and Auger Recombination in SrTiO(3). *Phys. Rev. B* **2008**, 77, 193202.

76. Pankove, J. I. *Optical Processes in Semiconductors*. Courier Corporation: 2012.

77. Zhang, Y. H.; Ding, C.; Wu, G. H.; Nakazawa, N.; Chang, J.; Ogomi, Y.; Toyoda, T.; Hayase, S.; KatayamA, K.; Shen, Q. Air Stable PbSe Colloidal Quantum Dot Heterojunction Solar Cells: Ligand-Dependent Exciton Dissociation, Recombination, Photovoltaic Property, and Stability. *J. Phys. Chem. C* **2016**, 120, 28509-28518.

78. Shen, Q.; Ogomi, Y.; Das, S. K.; Pandey, S. S.; Yoshino, K.; Katayama, K.; Momose, H.; Toyoda, T.; Hayase, S. Huge Suppression of Charge Recombination in P3HT-ZnO Organic-Inorganic Hybrid Solar Cells by Locating Dyes at the ZnO/P3HT Interfaces. *Phys. Chem. Chem. Phys.* **2013**, 15, 14370-14376.

79. Shen, Q.; Ogomi, Y.; Chang, J.; Tsukamoto, S.; Kukihara, K.; Oshima, T.; Osada, N.; Yoshino, K.; Katayama, K.; Toyoda, T.; Hayase, S. Charge Transfer and Recombination at the Metal Oxide/CH3NH3PbClI2/spiro-OMeTAD Interfaces: Uncovering the Detailed Mechanism Behind High Efficiency Solar Cells. *Phys. Chem. Chem. Phys.* **2014**, 16, 19984-19992.

80. Shen, Q.; Ogomi, Y.; Park, B. W.; Inoue, T.; Pandey, S. S.; Miyamoto, A.; Fujita, S.; Katayama, K.; Toyoda, T.; Hayase, S. Multiple Electron Injection Dynamics in Linearly-Linked Two Dye Co-Sensitized Nanocrystalline Metal Oxide Electrodes for Dye-Sensitized Solar Cells. *Phys. Chem. Chem. Phys.* **2012**, 14, 4605-4613.